

A two-strain COVID-19 co-infection model with strain 1 vaccination

Taqi A.M. Shatnawi ^a, Stephane Y. Tchoumi ^b, Herieth Rwezaura ^c, Khalid Dib ^d, Jean M. Tchuente ^e, Mo'tassem Al-arydah ^{d,*}

^a Department of Mathematics, Faculty of Science, The Hashemite University, P.O. Box 330127, Zarqa 13133, Jordan

^b Department of Mathematics and Computer Sciences ENSAL, University of Ngaoundéré, Cameroon

^c Mathematics Department, University of Dar es Salaam, Tanzania

^d Department of Mathematics, Khalifa University, Abu Dhabi, United Arab Emirates

^e School of Computer Science and Applied Mathematics, University of the Witwatersrand, Johannesburg, South Africa

ARTICLE INFO

Keywords:

COVID-19
Co-infection
Basic reproduction number
Equilibrium
Stability
Optimization

ABSTRACT

COVID-19 has caused substantial morbidity and mortality worldwide. Previous models of strain 1 vaccination with re-infection when vaccinated, as well as infection with strain 2 did not consider co-infected classes. To fill this gap, a two co-circulating COVID-19 strains model with strain 1 vaccination, and co-infected is formulated and theoretically analyzed. Sufficient conditions for the stability of the disease-free equilibrium and single-strain 1 and -strain 2 endemic equilibria are obtained. Results show as expected that (1) co-infected classes play a role in the transmission dynamics of the disease (2) a high efficacy vaccine could effectively help mitigate the spread of co-infection with both strain 1 and 2 compared to the low-efficacy vaccine. Sensitivity analysis reveals that the main drivers of the effective reproduction number R_e are primarily the effective contact rate for strain 2 (β_2), the strain 2 recovery rate (τ_2), and the vaccine efficacy or infection reduction due to the vaccine (η). Thus, implementing intervention measures to mitigate the spread of COVID-19 should not ignore the co-infected individuals who can potentially spread both strains of the disease.

1. Introduction

COVID-19, a highly contagious respiratory infection, spread rapidly when it first emerged.^{1,2} While the situation has improved with lower case numbers, updated booster vaccines, and fewer hospitalizations and deaths compared to the pandemic's peak, COVID-19 continues to pose risks. It remains a threat to the unvaccinated, those with disabilities, underlying health conditions, and individuals with weakened immune systems, including the elderly, immunocompetent, and immunocompromised.^{3–5} Additionally, some people, even with mild or no symptoms, may develop long COVID, a condition with lingering effects.³ Despite a lower mortality rate, the high number of hospitalizations underscores a significant global health burden and challenges for healthcare systems,⁶ with over one million COVID-19 deaths in the United States.³ As of October 14, 2023, the US COVID-19 positivity rate was 9.5%, with COVID-19 accounting for 2.5% of all deaths.⁷

COVID-19 transmission dynamics models have been investigated,^{8–23} this is list is far from exhaustive. The disease transmission rate in¹⁴ incorporates caution and sense of safety. Compartmental (deterministic) mathematical models are crucial to study the evolutionary dynamics of infectious diseases.²⁴ Such models which date as far

back as Bernoulli are characterized by the subdivision of the population into compartments based on individuals' health status.^{25–27} A second strain of a virus has the potential to substantially alter vaccine efficacy and transmission dynamics of the first strain. To this effect, mathematical modeling of a two-strain disease are not uncommon²⁸: malaria,²⁹ influenza,^{30,31} dengue,³² disease with age structure and super-infection,³³ influenza with a single vaccination,^{34,35} COVID-19^{16,21,36,37} to cite but a few and the references therein. In fact, two or multi-strain co-infections of COVID-19 could aggravate the clinical severity, increase the change in viral recombination, and pose a greater threat.³⁸ The number of strains could potentially increase logarithmically the maximum number of infected individuals and the mean mortality rate.³⁹ Co-infection is an impetus for recombination (which requires the coexistence of two COVID-19 strains in the same individual) between different COVID-19 variants.^{40–42} Because dual COVID-19 infection in the same patient was initially poorly described,^{43,44} only few studies to the best of our knowledge have considered two or multi-strain COVID-19 co-infection.

This study extends the existing two-strain COVID-19 models, which previously incorporated vaccination for strain 1 but overlooked co-

* Corresponding author.

E-mail address: motassem.alarydah@ku.ac.ae (M. Al-arydah).

Table 1
Description of the model's variables.

Variable	Description
$S(t)$	Susceptible individuals
$V_1(t)$	Vaccinated against COVID-19 type 1
$I_1(t)$	Infected with COVID-19 type 1
$I_2(t)$	Infected with COVID-19 type 2
$I_{12}(t)$	Infected with COVID-19 type 1 and 2
$R(t)$	Recovered individuals
λ_1	Force of infection of strain 2 when infected with strain 1
λ_2	Force of infection of strain 1 when infected with strain 2
λ_{S1}	Force of infection of strain 1 when susceptible
λ_{S2}	Force of infection of strain 2 when susceptible
λ_{V1}	Force of infection of strain 1 when vaccinated
λ_{V2}	Force of infection of strain 2 when vaccinated
λ_{S12}	Force of infection of dual infection when susceptible

infections.^{16,21,45} By including co-infected classes and considering non-permanent recovery,⁴⁶ this model addresses a significant gap, as re-infections and multi-strain dynamics have posed major challenges in managing COVID-19.⁴⁶ Unlike prior research, which often failed to account for the limited protection of strain 1 vaccination against the more virulent strain 2,^{36,47} this study integrates the dynamics of infections from both strains, providing a more comprehensive approach. Although simpler compared to more complex COVID-19 models, this study aims to better understand and address the impact of co-infections on the disease's dynamics.

The organization of this paper is as follows: Section 2 introduces a deterministic compartmental model for COVID-19 involving two strains and vaccination for strain 1. In Section 3, we perform a theoretical analysis of the model, covering equilibrium derivations, stability assessments, and calculations of the effective and basic reproduction numbers using standard dynamical systems methods. Section 4 provides model simulations and sensitivity analyses to validate the theoretical results. To manage disease spread, Section 5 reformulates the model as an optimal control problem and applies Pontryagin's Maximum Principle to identify the optimal control strategy. The paper concludes with a summary of the findings in Section 6.

2. Model formulation

We present a two-strain COVID-19 model that includes vaccination against strain 1. The total population, $N(t)$, is divided into six groups: susceptible individuals, $S(t)$, who increase due to constant recruitment Λ and decrease through vaccination (rate ν), natural death (rate μ), or infection by strain 1, strain 2, or both, with infection rates λ_{S1} , λ_{S2} , and λ_{S12} . The vaccinated group, $V_1(t)$, grows with new vaccinations and decreases due to natural death or infection with strain 2 at rate λ_V . Individuals infected with strain 1, $I_1(t)$, can also become infected with strain 2 (rate λ_1), recover at rate τ_1 , or die either naturally or due to COVID-19 (rate δ_1). Similarly, individuals infected with strain 2, $I_2(t)$, can become co-infected with strain 1 (rate λ_2), recover at rate τ_2 , or die from natural causes or COVID-19 (δ_2). Individuals infected with both strains, $I_{12}(t)$, recover at rate τ_{12} , or may die from natural causes or COVID-19 (δ_{12}). Finally, recovered individuals, $R(t)$, come from those who have recovered from infection, but this group decreases due to loss of immunity (rate σ) or natural death. The total population is expressed as $N(t) = S(t) + V_1(t) + I_1(t) + I_2(t) + I_{12}(t) + R(t)$. This model is based on the following assumptions:

- (a) Individuals mix evenly, meaning everyone has the same chance of getting infected when exposed to the disease.
- (b) Immunity after recovery is not permanent.
- (c) All susceptible individuals can be infected by either strain 1, strain 2, or both.
- (d) People vaccinated against strain 1 cannot be infected by both strains at once.

Table 2
Model parameters description.

Parameter	Description
Λ	Recruitment rate
β_1	Effective contact rate from strain 1
β_2	Effective contact rate from strain 2
β_{12}	Effective contact rate from strains 1 and 2
ν	Vaccination rate against strain 1 for susceptible individuals
μ	Natural death rate
σ	Rate of loss of infection-acquired immunity
τ_1	Recovery rate of infectious from strain 1
τ_2	Recovery rate of infectious from strain 2
τ_{12}	Recovery rate of infectious from strains 1 and 2
δ_1	Disease-induced death rate of infectious from strain 1
δ_2	Disease-induced death rate of infectious from strain 2
δ_{12}	Disease-induced death rate of infectious from both strains
η	Residual infectivity for vaccinated

- (e) Vaccination is accessible to everyone.

The compartment diagram illustrating the flow of the model is shown in Fig. 1. The definitions of the state variables and model parameters are provided in Tables 1 and 2, respectively.

Based on the information above and the model flow diagram in Fig. 1, we derive the following system of non-linear differential equations to describe the transmission dynamics of a two-strain COVID-19 model with vaccination.

$$\begin{aligned}
 \frac{dS}{dt} &= \Lambda - (\lambda_{S1} + \lambda_{S12} + \lambda_{S2} + \nu + \mu)S + \sigma R, \\
 \frac{dV_1}{dt} &= \nu S - (\lambda_{V1} + \lambda_{V2} + \mu)V_1, \\
 \frac{dI_1}{dt} &= \lambda_{S1}S + \lambda_{V1}V_1 - (\lambda_1 + \tau_1 + \delta_1 + \mu)I_1, \\
 \frac{dI_2}{dt} &= \lambda_{S2}S + \lambda_{V2}V_1 - (\lambda_2 + \tau_2 + \delta_2 + \mu)I_2, \\
 \frac{dI_{12}}{dt} &= \lambda_{S12}S + \lambda_1 I_1 + \lambda_2 I_2 - (\tau_{12} + \delta_{12} + \mu)I_{12}, \\
 \frac{dR}{dt} &= \tau_1 I_1 + \tau_2 I_2 + \tau_{12} I_{12} - (\mu + \sigma)R.
 \end{aligned} \tag{1}$$

with positive initial conditions $S(0) > 0$, $V_1(0) \geq 0$, $I_1(0) \geq 0$, $I_2(0) \geq 0$, $I_{12}(0) \geq 0$ and $R(0) \geq 0$, where λ_1 , λ_2 , λ_{S1} , λ_{S2} , λ_{S12} , λ_{V1} and λ_{V2} are define by

$$\begin{aligned}
 \lambda_{S1} &= \frac{\beta_1}{N}(I_1 + I_{12}), \quad \lambda_{S2} = \frac{\beta_2}{N}(I_2 + I_{12}), \quad \lambda_{S12} = \frac{\beta_{12}}{N}I_{12}, \\
 \lambda_{V1} &= \eta \frac{\beta_1}{N}(I_1 + I_{12}), \quad \lambda_{V2} = \frac{\beta_2}{N}(I_2 + I_{12}), \quad \lambda_1 = \frac{\beta_2}{N}I_2, \quad \lambda_2 = \frac{\beta_1}{N}I_1.
 \end{aligned}$$

Next,

$$\begin{aligned}
 \frac{dN}{dt} &= \Lambda - \mu N - \delta_1 I_1 - \delta_2 I_2 - \delta_{12} I_{12} \\
 &\leq \Lambda - \mu N.
 \end{aligned} \tag{2}$$

It can be shown that the feasible region

$$\Omega = \left\{ (S, V_1, I_1, I_2, I_{12}, R) \in \mathbb{R}_+^6 : N \leq \frac{\Lambda}{\mu} \right\}$$

is positively invariant and attracting with respect to the system given by (1).

3. Model analysis

In this section, we will explore the local stability of the disease-free equilibrium (DFE), focusing on when it remains stable or becomes unstable. We will also examine the conditions for the existence of an endemic equilibrium (EE), which shows how the disease can persist in the population over time. By analyzing these aspects, we aim to understand the dynamics of disease transmission and identify the key factors for controlling outbreaks.

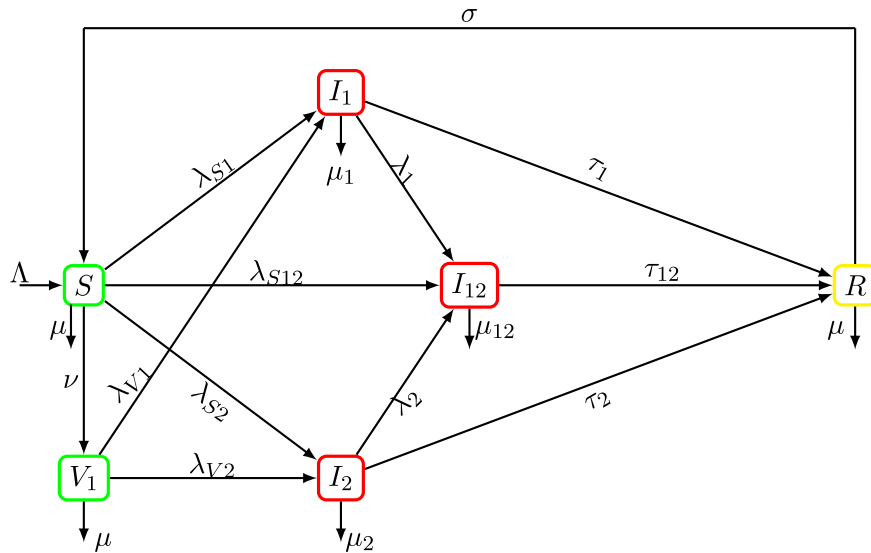


Fig. 1. Flow chart describing 2-strain transmission model of COVID-19, with $\mu_1 = \mu + \delta_1$, $\mu_2 = \mu + \delta_2$ and $\mu_{12} = \mu + \delta_{12}$.

3.1. Local stability of the disease-free equilibrium

The disease-free equilibrium of the system (1) is given by $E^0 = (S^0, V_1^0, I_1^0, I_2^0, I_{12}^0, R^0) = (\frac{\Lambda}{\nu + \mu}, \frac{\nu \Lambda}{\mu(\nu + \mu)}, 0, 0, 0, 0)$.

Using the next generation operator method,^{48,49} as introduced by Diekmann et al.,^{50,51} which involves calculating the spectral radius of the next generation operator and is denoted by $\mathcal{R}_e = \rho(FV^{-1})$, we compute the effective basic reproduction number (\mathcal{R}_e) for the model described by (1). This technique is also referenced in.⁵² The matrices representing the new infection terms, F , and the transition terms, V , from the model system (1) are given as follows.

$$F = \begin{pmatrix} \frac{\beta_1}{N^0}(S^0 + \eta V_1^0) & 0 & \frac{\beta_1}{N^0}(S^0 + \eta V_1^0) \\ 0 & \frac{\beta_2}{N^0}(S^0 + V_1^0) & \frac{\beta_2}{N^0}(S^0 + V_1^0) \\ 0 & 0 & \frac{\beta_{12}}{N^0}S^0 \end{pmatrix},$$

$$V = \begin{pmatrix} \tau_1 + \delta_1 + \mu & 0 & 0 \\ 0 & \tau_2 + \delta_2 + \mu & 0 \\ 0 & 0 & \tau_{12} + \delta_{12} + \mu \end{pmatrix}.$$

Hence, the effective/control reproduction number of the model (1) is given by the following expression:

$$\mathcal{R}_e = \max \left\{ \frac{\beta_1(\mu + \eta \nu)}{(\nu + \mu)(\tau_1 + \delta_1 + \mu)}, \frac{\beta_2(\mu + \nu)}{(\nu + \mu)(\tau_2 + \delta_2 + \mu)}, \frac{\beta_{12}\mu}{(\nu + \mu)(\tau_{12} + \delta_{12} + \mu)} \right\}.$$

Let

$$\mathcal{R}_1(\nu) = \frac{\beta_1(\mu + \eta \nu)}{(\nu + \mu)(\tau_1 + \delta_1 + \mu)}, \quad \mathcal{R}_2(\nu) = \frac{\beta_2(\mu + \nu)}{(\nu + \mu)(\tau_2 + \delta_2 + \mu)}, \quad \text{and}$$

$$\mathcal{R}_{12}(\nu) = \frac{\beta_{12}\mu}{(\nu + \mu)(\tau_{12} + \delta_{12} + \mu)}.$$

Then, the effective reproduction number is given as

$$\mathcal{R}_e = \max \{ \mathcal{R}_1(\nu), \mathcal{R}_2(\nu), \mathcal{R}_{12}(\nu) \},$$

which represents the average number of secondary infections caused by an infected individual in a population where some individuals are vaccinated. It is a critical threshold that helps determine whether an infectious disease will spread or decline in a population.

The basic reproduction number is obtain when $\nu = 0$, that is

$$\mathcal{R}_0 = \max \left\{ \frac{\beta_1}{\tau_1 + \delta_1 + \mu}, \frac{\beta_2}{\tau_2 + \delta_2 + \mu}, \frac{\beta_{12}}{\tau_{12} + \delta_{12} + \mu} \right\},$$

which represents the number of secondary infections in a fully susceptible population when there is no vaccine.

From⁵¹, the following result holds.

Theorem 1. The disease-free equilibrium $E^0 = (\frac{\Lambda}{\nu + \mu}, \frac{\nu \Lambda}{\mu(\nu + \mu)}, 0, 0, 0, 0)$ of the model (1) is locally asymptotically stable when $\mathcal{R}_e < 1$ and unstable when $\mathcal{R}_e > 1$.

Proof. The Jacobian matrix of the model system (1) at the DFE is given by equation given in Box I with $\phi_1 = \tau_1 + \delta_1 + \mu$, $\phi_2 = \tau_2 + \delta_2 + \mu$ and $\phi_{12} = \tau_{12} + \delta_{12} + \mu$.

The eigenvalues of the matrix J are

$$x_1 = -(\mu + \nu), \quad x_2 = -\mu, \quad x_3 = -(\sigma + \mu)$$

$$x_4 = (\mathcal{R}_1 - 1)\phi_1, \quad x_5 = (\mathcal{R}_2 - 1)\phi_2, \quad \text{and} \quad x_6 = (\mathcal{R}_{12} - 1)\phi_{12}.$$

Since x_1, x_2, x_3 are all negative, $\mathcal{R}_e < 1$, x_4, x_5 and x_6 are all negatives. Thus, when $\mathcal{R}_e < 1$, the DFE E^0 is locally asymptotically stable, and unstable otherwise. \square

Investigating the endemic equilibrium (EE) of the full model (1) can be quite complex. Therefore, we will simplify the analysis by examining two special cases: (1) COVID-19 strain 1 with vaccination and (2) COVID-19 strain 2 without vaccination.

3.2. Existence of endemic equilibrium strain 1 model

Theorem 2.

- (a) The COVID-19 strain 1 only with vaccination ($I_2 = 0$) admits a unique endemic equilibrium $\mathcal{E}_1^* = (S^*, V_1^*, I_1^*, 0, 0, R^*)$ iff $\mathcal{R}_1 > 1$.
- (b) The COVID-19 strain 2 only without vaccination ($I_1 = 0$) admits a unique endemic equilibrium $\mathcal{E}_2^* = (S^*, 0, 0, I_2^*, 0, R^*)$ iff $\mathcal{R}_2 > 1$.

Proof.

- (a) To find \mathcal{E}_1^* , we set the right hand sides of (1) equal to zero when $I_2 = 0$.

$$\Lambda - (\lambda_{S1}^* + \nu + \mu) S^* + \sigma R^* = 0, \tag{3}$$

$$\nu S^* - (\lambda_{V1}^* + \mu) V_1^* = 0, \tag{4}$$

$$J = \begin{pmatrix} -(\mu + \nu) & 0 & -\frac{\beta_1}{N^0} S^0 & -\frac{\beta_2}{N^0} S^0 & -\frac{S^0}{N^0} (\beta_1 + \beta_2 + \beta_{12}) & \sigma \\ \nu & -\mu & -\eta \frac{\beta_1}{N^0} V_1^0 & -\frac{\beta_2}{N^0} V_1^0 & -\frac{V_1^0}{N^0} (\eta\beta_1 + \beta_2) & 0 \\ 0 & 0 & \frac{\beta_1}{N^0} (S^0 + \eta V_1^0) - \phi_1 & 0 & \frac{\beta_1}{N^0} (S^0 + \eta V_1^0) & 0 \\ 0 & 0 & 0 & \frac{\beta_2}{N^0} (S^0 + V_1^0) - \phi_2 & \frac{\beta_2}{N^0} (S^0 + V_1^0) & 0 \\ 0 & 0 & 0 & 0 & \frac{\beta_{12}}{N^0} S^0 - \phi_{12} & 0 \\ 0 & 0 & \tau_1 & \tau_2 & \tau_{12} & -(\sigma + \mu) \end{pmatrix}.$$

Box I.

$$\lambda_{S1}^* S^* + \lambda_{V1}^* V_1^* - g_1 I_1^* = 0, \tag{5}$$

$$\tau_1 I_1^* - (\mu + \sigma) R^* = 0, \tag{6}$$

where $g_1 = \tau_1 + \delta_1 + \mu$,

$$\lambda_{S1}^* = \frac{\beta_1 I_1^*}{N^*} \quad \text{and} \quad \lambda_{V1}^* = \eta \lambda_{S1}^*. \tag{7}$$

Solving for S^*, V_1^*, I_1^* , and R^* in function of λ_{S1}^* , after some little algebraic manipulations, we obtain from (6),

$$R^* = \frac{\tau_1 I_1^*}{\mu + \sigma}, \tag{8}$$

from (4) and (5),

$$V_1^* = \frac{v g_1 I_1^*}{\lambda_{S1}^* (\eta \lambda_{S1}^* + \mu) + v \eta \lambda_{S1}^*}, \tag{9}$$

and

$$S^* = \frac{\lambda_{S1}^* (\eta \lambda_{S1}^* + \mu)}{v} V_1^*, \tag{10}$$

Substituting (8), (9) and (10) into (3) and solving for I_1^* , we obtain

$$I_1^* = \frac{\Lambda (\mu + \sigma) \lambda_{S1}^* (\eta \lambda_{S1}^* + v + \mu)}{\mu \lambda_{S1}^* g_1 (\lambda_{S1}^* (\eta + \mu) + \eta v) + \mu (\eta \lambda_{S1}^* + v + \mu) (g_1 (\mu + \sigma) + \sigma (\mu + \delta_1))}. \tag{11}$$

Adding Eqs. (3)–(6) and solving for N^* , we obtain

$$N^* = \frac{\Lambda - \delta_1 I_1^*}{\mu}. \tag{12}$$

By definition, $\lambda_{S1}^* = \frac{\beta_1 I_1^*}{N^*}$ and using (11) and (12) yields the following equation

$$\lambda_{S1}^* (a \lambda_{S1}^{*2} + b \lambda_{S1}^* + c) = 0, \tag{13}$$

where

$$a = -\eta \mu (\tau_1 + \mu + \sigma),$$

$$b = \eta (\mu + \sigma) (\eta \beta_1 - g_1 (2\mu + \nu)) + (\mu + \eta v) (\sigma \tau_1 + \delta_1),$$

$$c = \mu (\mu + \sigma) (\mu + v) g_1 (\mathcal{R}_1 - 1).$$

From Eq. (13), $\lambda_{S1} = 0$ which yields the DFE. The equation $a \lambda_{S1}^{*2} + b \lambda_{S1}^* + c = 0$ admits a unique non-negative solution when $\mathcal{R}_1 > 1$.

(b) To find \mathcal{E}_2^* when $I_1 = 0$, we set the right hand sides for the model (1) equal zero.

$$\Lambda - (\lambda_{S2}^* + \mu) S^* + \sigma R^* = 0, \tag{14}$$

$$\lambda_{S2}^* S^* - k_2 I_2^* = 0, \tag{15}$$

$$\tau_2 I_2^* - (\mu + \sigma) R^* = 0, \tag{16}$$

Table 3
Model parameter values.

Parameter	Sample value used	Unit	Reference
Λ	1000/(59 × 365)	humans × days ⁻¹	21
β_1	0.85 × 0.3	days ⁻¹	21
β_2	0.85 × 0.3	days ⁻¹	21
β_{12}	0.85 × 0.3	days ⁻¹	21
ν	0.9	days ⁻¹	21
μ	1/(59 × 365)	days ⁻¹	21
σ	1/90	days ⁻¹	21
τ_1	0.1	days ⁻¹	21
τ_2	0.1	days ⁻¹	21
τ_{12}	0.1	days ⁻¹	21
δ_1	0.0000683	days ⁻¹	21
δ_2	0.0000683	days ⁻¹	21
δ_{12}	0.0000683	days ⁻¹	21
η	0.13, 0.4	Unitless	Estimated

where $k_2 = \tau_2 + \delta_2 + \mu$ and $\lambda_{S2}^* = \frac{\beta_2 I_2^*}{N^*}$. After some computations similar to the case (a) above,

$$I_2^* = \frac{\Lambda \lambda_{S2}^* (\mu + \sigma)}{\mu k_2 (\lambda_{S2}^* + \mu) + \sigma (\lambda_{S2}^* (\mu + \delta_2) + \mu k_2)}, \tag{17}$$

$$R^* = \frac{\tau_2}{\mu + \sigma} I_2^*, \quad \text{and} \quad S^* = \frac{k_2 I_2^*}{\lambda_{S2}^*}, \tag{18}$$

where

$$\lambda_{S2}^* = \frac{k_2 (\mu + \sigma) (\mathcal{R}_2 - 1)}{2\tau_2 + \mu}.$$

$\lambda_{S2}^* > 0$ iff $\mathcal{R}_2 > 1$, and hence, the strain 2 COVID-19 without vaccination admits an endemic equilibrium when $\mathcal{R}_2 > 1$. □

4. Model simulations

In this section, we will estimate the time series solution and perform a sensitivity analysis of R_0 relative to the parameters. We will also formulate an optimal control problem and determine the optimal amount of vaccine needed to control the disease over a 100-day period.

4.1. Continuous time series solution and vaccine efficacy

To illustrate the fundamental mechanisms driving the model dynamics, we generated figures through numerical simulations to show the impact of different vaccine efficacy levels. The model parameters used are detailed in Table 3.

We simulate the model using MATLAB to visualize time series solutions for scenarios with both low and high vaccine efficacy against COVID-19 strain 1. Fig. 2 displays only the infective classes, with panels (a) and (b) representing low and high vaccine efficacy, respectively. As anticipated, a high-efficacy vaccine (residual infectivity $\eta = 0.13$) is more effective in reducing the spread of strain 1 and co-infection

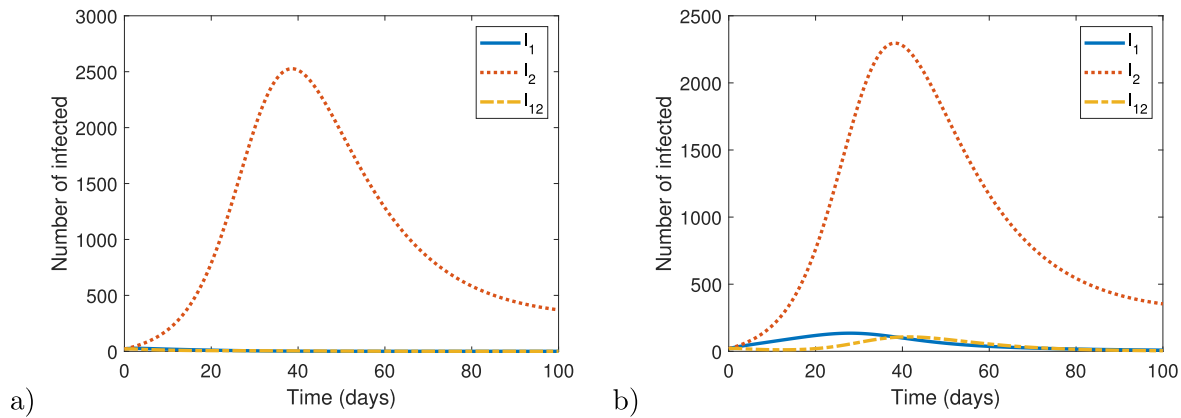


Fig. 2. Number of infected when applying vaccine with (a) residual infectivity $\eta = 0.13$, which implies $\mathcal{R}_0 = \mathcal{R}_2 = 0.3312$ (b) residual infectivity $\eta = 0.6$, which implies $\mathcal{R}_0 = \mathcal{R}_2 = 1.5283$.

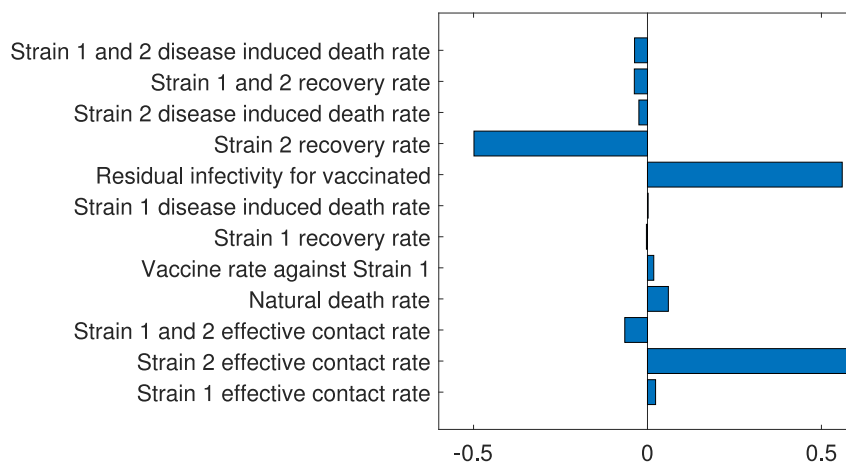


Fig. 3. Bar plots illustrate the sensitivity of R_e to each parameter. The longer the bar, the more influence that parameter has on R_e .

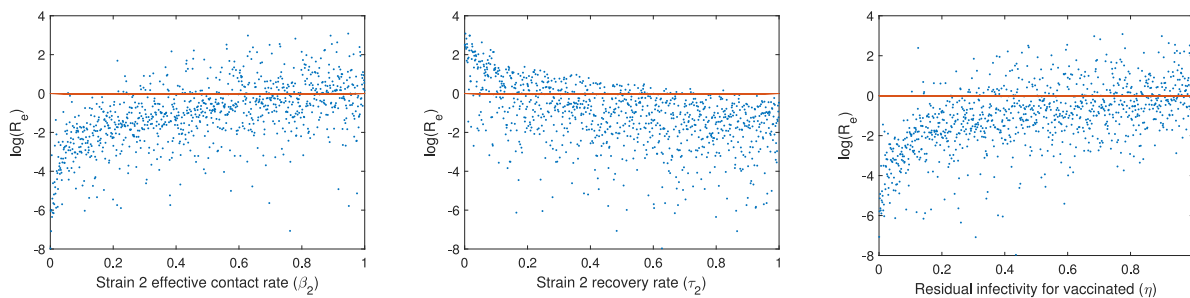


Fig. 4. Scatter plots displaying the PRCC values for each parameter.

compared to a low-efficacy vaccine (residual infectivity $\eta = 0.6$). However, both panels highlight the significance of considering co-infection in modeling COVID-19 dynamics—a key disease class that was not addressed in previous studies.^{16,21,45}

4.2. Sensitivity analysis: Parameter-induced variability in R_e

Given the uncertainty in parameter values, we perform a sensitivity analysis to see how changes in these parameters might affect the model’s effective basic reproduction number (initial disease spread). We use Latin Hypercube Sampling and partial rank correlation coefficients (PRCCs) for this analysis. Latin Hypercube Sampling helps explore how the outcome changes when input parameters vary, while PRCCs measure how sensitive the outcome is to each parameter, whether it increases or decreases. For more on this method, see.^{53,54}

Fig. 3 shows the PRCCs for each parameter. With μ constant, disease-induced mortality rates range from 0 to 0.05, and other parameters range from 0 to 1. Three key parameters affect the basic reproduction number (R_e): the contact rate for strain 2 (β_2), the recovery rate for strain 2 (τ_2), and the vaccine’s effect (η). Parameters with $PRCC > 0$ increase R_e when their values increase, while those with $PRCC < 0$ decrease R_e when their values increase. Small changes in β_2 , τ_2 , and η can significantly impact R_e , potentially shifting it from above one to below one. To manage COVID-19 effectively, it is crucial to reduce the contact rate for strain 2 (β_2), improve the recovery rate from strain 2 (τ_2), and ensure high vaccine efficacy against strain 1 (η). Fig. 4 is based on 1000 Monte Carlo simulations using parameters from specified ranges.

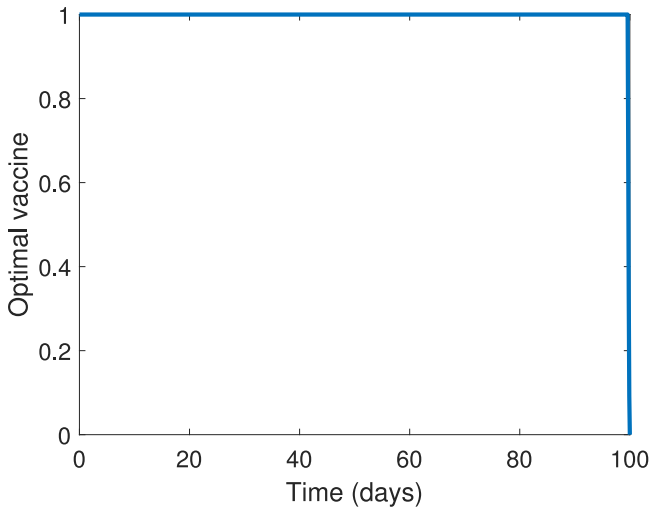


Fig. 5. Optimal vaccine with low efficacy.

5. Optimal control strategy

Public health policy and decision makers must make informed choices to effectively implement key intervention strategies and allocate resources.⁵⁵ Implementing control measures is essential for selecting the best approach to managing infectious diseases.^{54,56–58} In this regard, we consider vaccination against COVID-19 strain 1 and introduce $u(t)$, a time-dependent control variable, to replace the constant vaccination rate v . If $u(t)$ is an integrable function of time, we can define the total cost functional for a finite vaccine and implementation period T . This leads us to develop an optimal control model incorporating this time-dependent control variable.

$$J(u) = \int_0^T \left(A_1 I_1 + A_2 I_2 + A_{12} I_{12} + \frac{A_u}{2} (u(t))^2 \right) dt \tag{19}$$

To balance the terms in the cost functions, we use the constants A_1, A_2, A_{12} , and A_u as weights. The choice of non-linear control efforts is made for technical reasons, while the quadratic control function helps manage the logistics of delivering large quantities of vaccines.

To establish the necessary conditions for the optimal control u^* , we utilize Pontryagin’s maximum principle,⁵⁹ which provides a fundamental mathematical approach for this analysis.

$$J(u^*) = \min_{u \in \mathbb{V}} J(u), \tag{20}$$

in the feasible region

$$\mathbb{V} = \{u : 0 \leq u \leq 1\},$$

with u being a Lebesgue measurable function. Here’s an alternative version:

Consequently, we minimize pointwise the Hamiltonian

$$H = A_1 I_1 + A_2 I_2 + A_{12} I_{12} + \frac{A_u}{2} (u(t))^2 + \sum_{i=1}^6 p_i(t) g_i, \tag{21}$$

where $p_i, g_i, i = 1, 2, \dots, 6$ represent the adjoint functions and the right-hand sides of the system equations, respectively.

According to,⁶⁰ if the optimal control u^* and the corresponding state ϕ^* form an optimal pair, then there must exist a non-trivial adjoint vector $p = (p_1, p_2, \dots, p_6)$ that satisfies the following conditions:

$$\begin{cases} \frac{d\phi}{dt} = \frac{\partial H(\phi, u, \lambda)}{\partial \lambda}, \\ \frac{dp}{dt} = -\frac{\partial H(\phi, u, p)}{\partial \phi}, \\ \frac{\partial H(\phi, u, p)}{\partial u} = 0, \end{cases}$$

$S(0)$	10,000
$V_1(0)$	2
$I_1(0)$	20
$I_2(0)$	20
$I_{12}(0)$	20
$R_0(0)$	0

which after derivation implies

$$\begin{cases} u^* = 0, & \text{if } \frac{\partial H}{\partial u} < 0, \\ 0 \leq u^* \leq 1, & \text{if } \frac{\partial H}{\partial u} = 0, \\ u^* = 1, & \text{if } \frac{\partial H}{\partial u} > 0. \end{cases}$$

with $C_i, i = 1, 2, \dots, 6$ given in the Appendix, the following theorem regarding the necessary conditions for the Hamiltonian is applicable.

Theorem 3. Consider an optimal control u^* and the corresponding solution ϕ^* for the state Eq. (1). There exists an adjoint vector p that satisfies the following adjoint system of equations:

$$\frac{dp_i}{dt} = C_i, i = 1, 2, \dots, 6, \tag{22}$$

where $p_i(T) = 0, i = 1, 2, \dots, 6$ represents the transversality condition at the final time T . Additionally, the optimal control u^* is given by

$$u^* = \min \left\{ \max \left\{ \frac{(p_1 - p_2)S}{A_u}, 0 \right\}, 1 \right\}. \tag{23}$$

Proof. Here’s a completely rephrased version:

The adjoint system of equations is derived by differentiating the Hamiltonian (21) with respect to ϕ (using Mathematica software). This gives the equation $\frac{dp}{dt} = -\frac{\partial H(\phi, u, p)}{\partial \phi}$, with transversality conditions $p(T) = 0$ at the final time T .

The optimal control u^* is derived by applying the optimality condition $\frac{\partial H}{\partial u} = 0$ to the Hamiltonian. This condition yields:

$$\frac{\partial H}{\partial u} = uA_u - Sp_1 + Sp_2 = 0 \Rightarrow u^* = \frac{(p_1 - p_2)S}{A_u}.$$

By utilizing the properties of the control space \mathbb{V} , the control can be expressed as follows:

$$u^* = \begin{cases} 0, & \text{if } (p_1 - p_2)S < 0, \\ u_1^*, & \text{if } 0 \leq (p_1 - p_2)S \leq A_u, \\ 1, & \text{if } (p_1 - p_2)S > A_u. \end{cases}$$

This can be expressed in a more compact form as given in Eq. (23). \square

Next, we examine the second derivative of the Hamiltonian $\frac{\partial^2 H}{\partial u^2} > 0$. Since,

$$\frac{\partial^2 H}{\partial u^2} = A_u > 0,$$

the optimal control is indeed a minimization.

5.1. Estimating optimal solution

To estimate the optimal solution, we employ the forward-backward sweep method described in,⁶⁰ combined with the Runge-Kutta fourth-order technique⁶¹ to solve Eq. (20) under the initial conditions specified in Table 4, while incorporating the vaccine rate $u(t)$. Similar techniques can be found in.^{62,63} Numerical simulations are then conducted to determine the optimal amount of vaccine required to manage COVID-19 within a finite time period. The process begins with an initial control guess of $v = 0$ using the parameter values listed in Table 3 and the initial conditions provided in Table 4. The weight constants are assumed to be $A_1 = 1000, A_2 = 1000, A_{12} = 2000$, and $A_u = 30$.

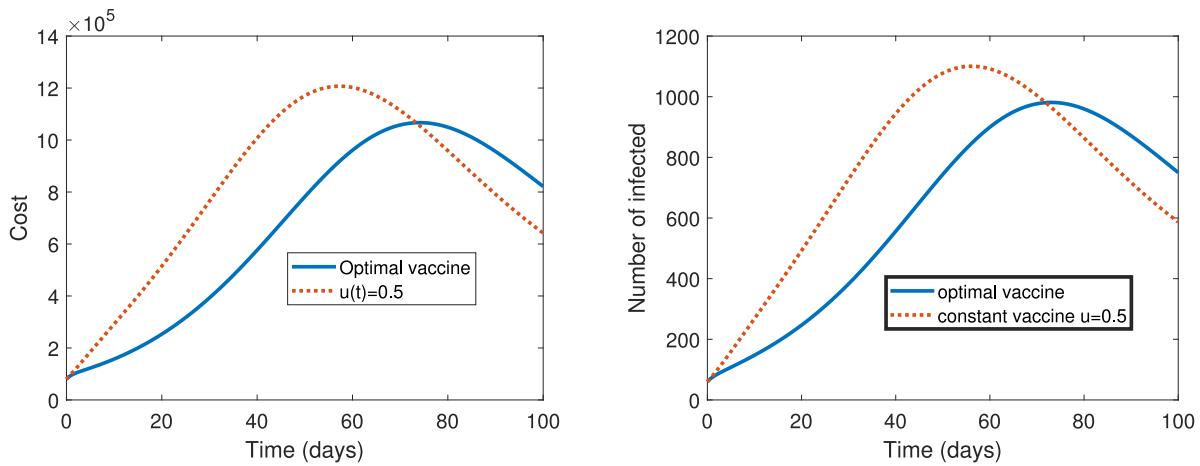


Fig. 6. Left panel: the cost of the vaccination campaign. Right panel: time evolution of the number of infected for both optimal vaccine ($u^*(t) = 1$) and constant vaccine ($u = 0.5$).

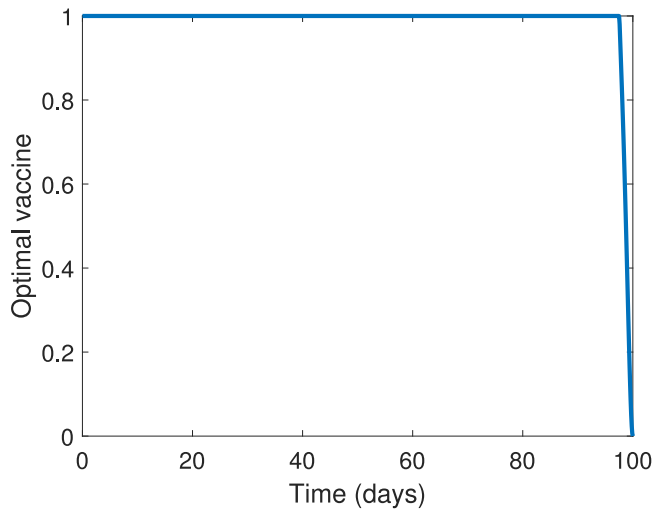


Fig. 7. Optimal vaccine with high efficacy.

The MATLAB simulation code operates as follows: First, the fourth-order Runge–Kutta method is employed to solve Eq. (1) using the initial conditions specified in Table 4 with the period $T = 100$ days, and step size 0.01. The resulting state values are then used to solve the adjoint Eqs. (22). These adjoint equations, with final conditions set to zero, are solved backward in time using the same fourth-order Runge–Kutta method. The solutions to these adjoint equations are then applied to update the controls as specified in Eq. (23). This iterative process continues until the current state, adjoint, and control values converge sufficiently close to the values from the previous iteration. Finally, the optimal vaccination levels required for the two scenarios are determined.

(1) **Low vaccine efficacy $\eta = 30\%$**

Fig. 5 displays the optimal vaccination strategy $u^*(t)$, highlighting the need for full vaccine coverage throughout the entire 100-day period, where $u^*(t) = 1$. Panels on the left and right in Fig. 6 compare the costs and infection rates under two scenarios: the optimal vaccination strategy and a constant vaccination approach with $u(t) = 0.5$. It is clear that the optimal strategy markedly

decreases both the number of infections and the associated costs compared to the constant vaccination approach.

(2) **High vaccine efficacy $\eta = 13\%$**

Fig. 7 illustrates the optimal vaccination strategy $u^*(t)$. It shows that full vaccine coverage at $u^*(t) = 1$, is crucial for the first 98 days with coverage gradually decreasing to zero by day 100. Figs. 8(a) and (b) present a comparative analysis of both costs and infection rates, for the optimal vaccination strategy and a constant vaccination approach with $u(t) = 0.5$. The results clearly demonstrate that the optimal vaccination strategy leads to a significant reduction in both the number of infections and associated costs compared to the constant vaccination approach.

6. Conclusion

COVID-19 spread rapidly worldwide when it emerged and has caused significant morbidity and mortality, as well as economic hardship. Very effective vaccines have been developed, but when first deployed, other highly infectious variants of the disease for which these vaccines were less or not effective started emerging. In, ^{16,21} 2-strain of COVID-19 models are formulated, but the models did not account for the co-infected classes. To fill this gap, the present study included individuals co-infected with both COVID-19 strains 1 and 2. Standard routine theoretical analysis of the model is presented: The effective reproduction number \mathcal{R}_e is derived using the next generation matrix approach. The disease-free equilibrium is stable if $\mathcal{R}_e < 1$, and unstable otherwise. The complexity of the proposed model preclude the investigation of the stability of the endemic equilibrium of the full model, and for this reason, only the sub-models endemic equilibria are analyzed. Whenever $\mathcal{R}_1 > 1$, and $\mathcal{R}_2 > 1$, strain 1 only, respectively strain 2 only has a unique and stable endemic equilibrium.

The model simulations as expected support the fact that highly effective vaccination helps to mitigate the spread of COVID-19 strain 1 and the co-circulation of strains 1 and 2 in a considerably shorter time frame compared to the low-efficacy vaccine. Thus, individuals harboring both strains of the disease should be given prominence as neglecting the co-infected class could be a drawback in the implementation of intervention measures, especially when multiple strains are co-circulating. Sensitivity analysis reveals that the main drivers of the effective reproduction number \mathcal{R}_e are primarily the effective contact rate for strain 2 (β_2), the strain 2 recovery rate (τ_2), and the infection reduction due to the vaccine (η). This results agrees with the findings in¹⁶ that implementation of intervention measures targeting contact

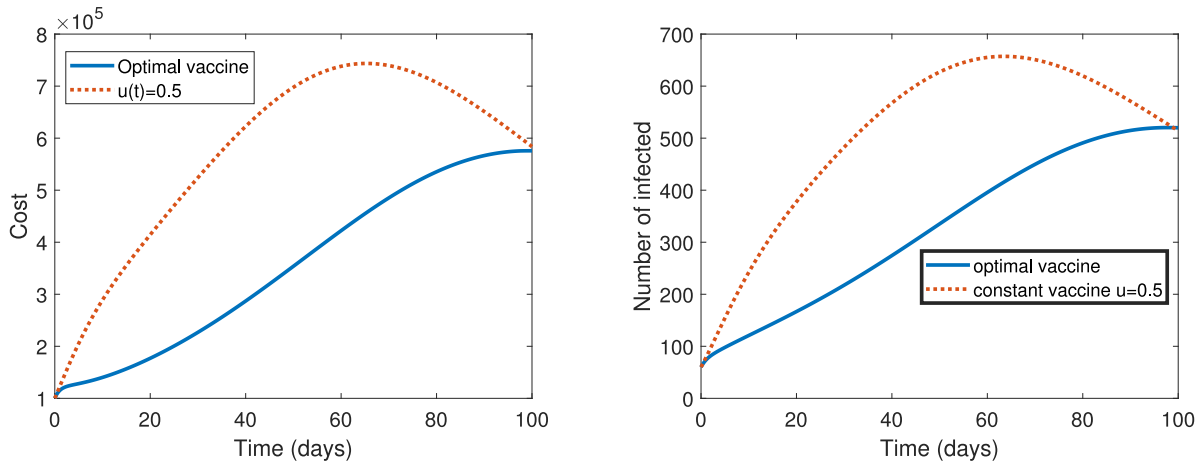


Fig. 8. Left panel: cost of vaccine. Right panel: number of infected for both optimal vaccine and constant vaccine ($u = 0.5$).

reduction (e.g., social distancing), mass vaccination and treatment will greatly help in curbing the spread of the disease.

The model has some limitations, which include, but are not limited to, the assumption of homogeneous mixing within the population. This assumption simplifies the analysis but may not accurately capture the complexities of real-world interactions influenced by factors such as geography, age, and social behavior.

The proposed model which is not exhaustive could be extended to include the more than one strain (multiple) strain of COVID-19, with all the vaccination boosters (3 booster after the first dose) since a single dose of the vaccine proved not sufficient to control the rapid spread.

Declaration of competing interest

The authors declare that they have no conflict of interest.

Data availability

No data was used for the research described in the article.

Appendix

After some algebraic calculations,

$$\begin{aligned}
 C_1 &= p_1(\mu + u - S \frac{\beta_1(I_1 + I_{12}) + \beta_2(I_2 + I_{12}) + I_{12}\beta_{12}}{N^2} \\
 &\quad + \frac{\beta_1(I_1 + I_{12}) + \beta_2(I_2 + I_{12}) + I_{12}\beta_{12}}{N}) \\
 &\quad - p_2(u + V_1 \frac{\beta_2(I_2 + I_{12}) + \beta_1\eta(I_1 + I_{12})}{N^2}) \\
 &\quad - p_3(\frac{\beta_1(I_1 + I_{12})}{N} - \frac{\beta_1 S(I_1 + I_{12})}{N^2} + \frac{I_1 I_2 \beta_2}{N^2} - \frac{V_1 \beta_1 \eta(I_1 + I_{12})}{N^2}) \\
 &\quad - p_4(\frac{\beta_2(I_2 + I_{12})}{N} - \frac{\beta_2(S + V_1)(I_2 + I_{12})}{N^2} + \frac{I_1 I_2 \beta_1}{N^2}) \\
 &\quad + p_5(\frac{I_1 I_2 \beta_1}{N^2} - \frac{I_{12} \beta_{12}}{N} + \frac{I_1 I_2 \beta_2}{N^2} + \frac{I_{12} S \beta_{12}}{N^2}), \\
 C_2 &= -p_1 S \frac{\beta_1(I_1 + I_{12}) + \beta_2(I_2 + I_{12}) + I_{12}\beta_{12}}{N^2} \\
 &\quad + p_2(\mu - V_1 \frac{\beta_2(I_2 + I_{12}) + \beta_1\eta(I_1 + I_{12})}{N^2} + \frac{\beta_2(I_2 + I_{12}) + \beta_1\eta(I_1 + I_{12})}{N}) \\
 &\quad + p_3(\frac{S\beta_1(I_1 + I_{12}) - I_1 I_2 \beta_2 + V_1 \beta_1 \eta(I_1 + I_{12})}{N^2} - \frac{\beta_1 \eta(I_1 + I_{12})}{N}) \\
 &\quad - p_4(\frac{\beta_2(I_2 + I_{12})}{N} - \frac{\beta_2(S + V_1)(I_2 + I_{12}) - I_1 I_2 \beta_1}{N^2}) \\
 &\quad + p_5(\frac{I_1 I_2 \beta_1 + I_1 I_2 \beta_2 + I_{12} S \beta_{12}}{N^2}),
 \end{aligned}$$

$$\begin{aligned}
 C_3 &= -A_1 - p_1 S(-\frac{\beta_1}{N} + \frac{\beta_1(I_1 + I_{12}) + \beta_2(I_2 + I_{12}) + I_{12}\beta_{12}}{N^2}) \\
 &\quad - p_2 V_1(-\frac{\beta_1 \eta}{N} + \frac{\beta_2(I_2 + I_{12}) + \beta_1 \eta(I_1 + I_{12})}{N^2}) \\
 &\quad + p_3(\delta_1 + \mu + \tau_1 + \frac{I_2 \beta_2 - S \beta_1 - V_1 \beta_1 \eta}{N} \\
 &\quad \quad + \frac{S \beta_1(I_1 + I_{12}) - I_1 I_2 \beta_2 + V_1 \beta_1 \eta(I_1 + I_{12})}{N^2}) \\
 &\quad + p_4(\frac{I_2 \beta_1}{N} - \frac{I_1 \beta_1 - \beta_2(S + V_1)(I_2 + I_{12})}{N^2}) \\
 &\quad + p_5(\frac{I_1 I_2 \beta_1 + I_1 I_2 \beta_2 + I_{12} S \beta_{12}}{N^2} - \frac{I_2 \beta_2 + I_2 \beta_1}{N}) - p_6 \tau_1, \\
 C_4 &= -A_2 - p_1 S(\frac{\beta_1(I_1 + I_{12}) + \beta_2(I_2 + I_{12}) + \beta_{12} I_{12}}{N^2} - \frac{\beta_2}{N}) \\
 &\quad - p_2 V_1(\frac{\beta_2(I_2 + I_{12}) + \beta_1 \eta(I_1 + I_{12})}{N^2} - \frac{\beta_2}{N}) \\
 &\quad + p_3(\frac{I_1 \beta_2}{N} + \frac{S \beta_1(I_1 + I_{12}) + V_1 \beta_1 \eta(I_1 + I_{12}) - I_2 \beta_2}{N^2}) \\
 &\quad + p_4(\delta_2 + \mu + \tau_2 - \frac{\beta_2(S + V_1) - I_1 \beta_1}{N} + \frac{\beta_2(S + V_1)(I_2 + I_{12}) - I_1 I_2 \beta_1}{N^2}) \\
 &\quad + p_5(\frac{I_1 I_2 \beta_1 + I_1 I_2 \beta_2 + I_{12} S \beta_{12}}{N^2} - \frac{I_1 \beta_1 + I_1 \beta_1}{N}) - p_6 \tau_2, \\
 C_5 &= -A_{12} + p_1 S(\frac{\beta_1 + \beta_2 + \beta_{12}}{N} - \frac{\beta_1(I_1 + I_{12}) + \beta_2(I_2 + I_{12}) + I_{12}\beta_{12}}{N^2}) \\
 &\quad + p_2 V_1(\frac{\beta_2 + \beta_1 \eta}{N} - \frac{\beta_2(I_2 + I_{12}) + \beta_1 \eta(I_1 + I_{12})}{N^2}) \\
 &\quad - p_3(\frac{S \beta_1 + V_1 \beta_1 \eta}{N} + \frac{I_1 I_2 \beta_2 - S \beta_1(I_1 + I_{12}) - V_1 \beta_1 \eta(I_1 + I_{12})}{N^2}) \\
 &\quad - p_4(\frac{\beta_2(S + V_1)}{N} - \frac{\beta_2(S + V_1)(I_2 + I_{12}) - \beta_1 I_1 I_2}{N^2}) \\
 &\quad + p_5(\delta_{12} + \mu + \tau_{12} - \frac{S \beta_{12}}{N} + \frac{\beta_1 I_1 I_2 + \beta_2 I_1 I_2 + \beta_{12} I_{12} S}{N^2}) - p_6 \tau_{12}, \\
 C_6 &= -p_1(\sigma + S \frac{\beta_1(I_1 + I_{12}) + \beta_2(I_2 + I_{12}) + I_{12}\beta_{12}}{N^2}) \\
 &\quad - p_2 V_1(\frac{\beta_2(I_2 + I_{12}) + \beta_1 \eta(I_1 + I_{12})}{N^2}) \\
 &\quad + p_3(\frac{S \beta_1(I_1 + I_{12}) - I_1 I_2 \beta_2 + V_1 \beta_1 \eta(I_1 + I_{12})}{N^2}) \\
 &\quad + p_4(\frac{\beta_2(S + V_1)(I_2 + I_{12}) - (I_1 I_2 \beta_1)}{N^2}) \\
 &\quad + p_5(\frac{I_1 I_2 \beta_1 + I_1 I_2 \beta_2 + I_{12} S \beta_{12}}{N^2}).
 \end{aligned}$$

References

1. World Health Organization, et al Coronavirus disease 2019 (Covid-19): Situation report. 2020. 67.

2. Li Qun, Guan Xuhua, Wu Peng, et al Early transmission dynamics in Wuhan, China, of novel Coronavirus-infected pneumonia. *N Engl J Med.* 2020.
3. <https://www.cdc.gov/coronavirus/2019-ncov/your-health/about-covid-19.html>.
4. Vital Surveillances. The epidemiological characteristics of an outbreak of 2019 novel Coronavirus diseases (Covid-19)-China, 2020. *China CDC Weekly.* 2020;2(8):113–122.
5. Lueking R, Clark AE, Narasimhan M, et al SARS-CoV-2 coinfections with variant genomic lineages identified by multiplex fragment analysis. *Front Genet.* 2022;13:942713.
6. Wu Z, McGoogan JM. Characteristics of and important lessons from the coronavirus disease 2019 (covid-19) outbreak in China: Summary of a report of 72 314 cases from the Chinese center for disease control and prevention. *JAMA.* 2020.
7. CDC <https://covid.cdc.gov/covid-data-tracker/#datatracker-home>.
8. DarAssi MH, Ahmad I, Meetei MZ, Alsulami M, Khan MA, Tag-eldin EM. The impact of the face mask on SARS-CoV-2 disease: Mathematical modeling with a case study. *Results Phys.* 2023;51:106699.
9. DarAssi MH, Damrah S, AbuHour Y. A mathematical study of the omicron variant in a discrete-time Covid-19 model. *Eur Phys J Plus.* 2023;138:601.
10. DarAssi MH, Shatnawi TAM, Safi MA. Mathematical analysis of a MERS-Cov Coronavirus model. *Demonstratio Math.* 2022;55(1):265–276.
11. Forrest O, Al-arydah M. Optimal control strategies for infectious diseases with consideration of behavioral dynamics. *Math Methods Appl Sci.* 2024;1–19. <http://dx.doi.org/10.1002/mma.10388>.
12. Al-arydah M. Assessing vaccine efficacy for infectious diseases with variable immunity using a mathematical model. *Sci Rep.* 2024;14:18572.
13. Al-arydah M, Berhe H, Dib K, Madhu K. Mathematical modeling of the spread of the coronavirus under strict social restrictions. *Math Methods Appl Sci.* 2021;1–11. <http://dx.doi.org/10.1002/mma.7965>.
14. Al-arydah M. Mathematical modeling and optimal control for COVID-19 with population behavior. *Math Methods Appl Sci.* 2023;46:19184–19198. <http://dx.doi.org/10.1002/mma.9619>.
15. DarAssi Mahmoud H, Ahmad Irfan, Meetei Mutum Zico, Alsulami Mansoor, Khan Muhammad Altaf, Tag-eldin Elsayed M. The impact of the face mask on SARS-CoV-2 disease: Mathematical modeling with a case study. *Results Phys.* 2023;51:106699. <http://dx.doi.org/10.1016/j.rinp.2023.106699>,
16. Tchoumi SY, Rwezaura H, Tchuente JM. Dynamic of a two-strain COVID-19 model with vaccination. *Results Phys.* 2022;39:105777.
17. Pedro SA, Ndjomatchoua FT, Jentsch P, Tchuente JM, Anand M, Bauch CT. Conditions for a second wave of COVID-19 due to interactions between disease dynamics and social processes. *Front Phys.* 2020;8:574514.
18. Jentsch PC, Anand M, Bauch CT. Prioritising COVID-19 vaccination in changing social and epidemiological landscapes: A mathematical modelling study. *Lancet Infect Dis.* 2021. [http://dx.doi.org/10.1016/S1473-3099\(21\)00057-8](http://dx.doi.org/10.1016/S1473-3099(21)00057-8).
19. Olumuyiwa JP, Qureshi S, Yusuf A, Al-Shomrani M, Idowu AA. A new mathematical model of COVID-19 using real data from Pakistan. *Results Phys.* 2021;24:104098.
20. Buckner JH, Chowell G, Springborn MR. Dynamic prioritization of COVID-19 vaccines when social distancing is limited for essential workers. *Proc Natl Acad Sci.* 2021;118(16):e2025786118.
21. de Leon UA, Avila-Vales E, Huang KL. Modeling COVID-19 dynamic using a two-strain model with vaccination. *Chaos Solitons Fractals.* 2022;157:111927.
22. Rajput A, Sajid M, Tanvi, et al Optimal control strategies on COVID-19 infection to bolster the efficacy of vaccination in India. *Sci Rep.* 2021;11. Article No. 20124. October 11.
23. Al-arydah M. *Choosing between vaccine efficacy and vaccine price: A mathematical model for COVID-19.* Birkhäuser, Cham: Trends in Mathematics; 2024. http://dx.doi.org/10.1007/978-3-031-41420-6_9.
24. Olivares A, Staffetti E. Uncertainty quantification of a mathematical model of COVID-19 transmission dynamics with mass vaccination strategy. *Chaos Solitons Fractals.* 2021;146:110895.
25. Bernoulli D. Essai d'une nouvelle analyse de la mortalitecausee par la petite verole et des avantages de l'inoculation pour la prevenir. *Me m Math Phys Acad R Sci Paris.* (1766):1–45.
26. Kermack WO, McKendrick AG. A contribution to the mathematical theory of epidemics. *Proc R Soc Lond Ser A.* 1927;115(772):700–721.
27. Dietz K, Heesterbeek JAP. Daniel Bernoulli's epidemiological model revisited. *Math Biosci.* 2002;180(1–2):1–21.
28. Nuno M, Castillo-Chavez C, Feng Z, Martcheva M. Mathematical models of influenza: The role of cross-immunity, quarantine and age-structure. In: Brauer F, van den Driessche P, Wu J, eds. *Mathematical epidemiology.* Berlin, Heidelberg: Springer; 2008. In: Lecture notes in mathematics; vol. 1945.
29. Bala S, Gimba B. Global sensitivity analysis to study the impacts of bed-nets, drug treatment, and their efficacies on a two-strain Malaria model. *Math Comput Appl.* 2019;24(1):32.
30. Chung KW, Lui R. Dynamics of two-strain influenza model with cross-immunity and no quarantine class. *J Math Biol.* 2016;73(6–7):1467–1489.
31. Chamchod F, Britton NF. On the dynamics of a two-strain influenza model with isolation. *Math Model Nat Phenom.* 2012;7(3):49–61.
32. Rashkov P. BW Kooi complexity of host-vector dynamics in a two-strain Dengue model. *J Biol Dyn.* 2021;15(1):35–72.
33. Li XZ, Liu JX, Martcheva M. An age-structured two-strain epidemic model with super-infection. *Math Biosci Eng.* 2010;7(1):123–147.
34. Nic-May AJ, Avila-Vales EJ. Global dynamics of a two-strain flu model with a single vaccination and general incidence rate. *Math Biosci Eng.* 2020;17(6):7862–7891.
35. Rahman SM Ashrafur. X Zou Flu epidemics: A two-strain flu model with a single vaccination. *J Biol Dyn.* 2011;5(5):376–390.
36. Gonzalez-Parra G, Martinez-Rodriguez D, Villanueva-Mico RJ. Impact of a new SARS-CoV-2 variant on the population: A mathematical modeling approach. *Math Comput Appl.* 2021;26(2):25.
37. Yang W, Shaman J. COVID-19 pandemic dynamics in India, the SARS-CoV-2 Delta variant and implications for vaccination. *J R Soc Interface.* 2022;191:20210900.
38. Li Y, et al Both simulation and sequencing data reveal coinfections with multiple SARS-CoV-2 variants in the COVID-19 pandemic. *Comput Struct Biotechnol J.* 2022;20:1389–1401.
39. Lazebnik T, Bunimovich-Mendrazitsky S. Generic approach for mathematical model of multi-strain pandemics. *PLoS One.* 2022;17(4):e0260683.
40. Penas-Utrilla D, Perez-Lago L, Molero-Salinas A, et al Systematic genomic analysis of SARS-CoV-2 co-infections throughout the pandemic and segregation of the strains involved. *Genome Med.* 2023;15:57.
41. He Y, Ma W, Dang S, et al Possible recombination between two variants of concern in a COVID-19 patient. *Emerg Microbes Infect.* 2022;11(1):552–555.
42. Jackson B, Boni MF, Bull MJ, et al Generation and transmission of interlineage recombinants in the SARS-CoV-2 pandemic. *Cell.* 2021;184(20):5179–5188. e8.
43. Samoilov AE, Kaptelova VV, Bukharina AY, et al Case report: Change of dominant strain during dual SARS-CoV-2 infection. *BMC Infect Dis.* 2021;21(1):959.
44. Vatteroni ML, Capria AL, Spezia PG, Frateschi S, Pistello M. Co-infection with SARS-CoV-2 Omicron BA.1 and BA.2 subvariants in a non-vaccinated woman. *Lancet Microbe.* 2022;3(7):e478.
45. Martsenyuk V, Bernas M, Klos-Witkowska A. Two-strain COVID-19 model using delayed dynamic system and big data. *IEEE Access.* 2021;9:113866–113878.
46. Arruda EF, Das SS, Dias CM, Pastore DH. Modelling and optimal control of multi strain epidemics, with application to COVID-19. *PLoS One.* 2021;16(9):e0257512.
47. Puga GF, Monteiro LHA. The co-circulation of two infectious diseases and the impact of vaccination against one of them. *Ecol Complex.* 2021;47:100941.
48. Anderson RM, May RM. *Population biology of infectious diseases.* Berlin, Heidelberg, New York: Springer-Verlag; 1982.
49. Heffernan JR, Smith RJ, Wahl LM. Perspective on the basic reproductive ratio. *J R Soc Interface.* 2005;2:281–293.
50. Diekmann O, Heesterbeek JAP, Metz JAJ. On the definition and the computation of the basic reproduction ratio R_0 in models for infectious diseases. *J Math Biol.* 1990;35:503–522.
51. van den Driessche P, Watmough J. Reproduction numbers and sub-threshold endemic equilibria for compartmental models of disease transmission. *Math Biosci.* 2002;180:29–48.
52. Al-arydah M, Smith RJ. Adding education to test and treat: Can we overcome drug resistance? *J Appl Math.* 2015;2015. <http://dx.doi.org/10.1155/2015/781270>.
53. Blower SM, Dowlatabadi H. Sensitivity and uncertainty analysis of complex models of disease transmission: An HIV model, as an example. *Int Stat Rev.* 1994;62(2):229–243.
54. Tchoumi SY, Chukwu CW, Diagne ML, Rwezaura H, Juga ML, Tchuente JM. Optimal control of a two-group malaria transmission model with vaccination. *New Model Anal Health Inform Bioinform.* 2023;12:7.
55. Sooknanan J, Seemungal TAR. Criminals and their models - A review of epidemiological models describing criminal behaviour. *Appl Math Comput.* 2023;458:128212.
56. Rwezaura H, Diagne ML, Omame A, de Espindola AL, Tchuente JM. Mathematical modeling and optimal control of SARS-CoV-2 and tuberculosis co-infection: A case study of Indonesia. *Model Earth Syst Environ.* 2022;8:5493–5520.
57. Ringa N, Diagne ML, Rwezaura H, Omame A, Tchoumi SY, Tchuente JM. HIV and COVID-19 co-infection: A mathematical model and optimal control. *Inform Med Unlocked.* 2022;31:100978.
58. Goudiaby MS, Gning LD, Diagne ML, Dia BM, Rwezaura H, Tchuente JM. Optimal control analysis of a COVID-19 and tuberculosis co-dynamics model. *Inform Med Unlocked.* 2022;28:100849.
59. Pontryagin LS, Boltyanskii VG, Gamkrelidze RV, Mishchenko EF. *The mathematical theory of optimal processes.* New York: Wiley; 1962.
60. Lenhart S, Workman JT. *Optimal control applied to biological models.* Chapman and Hall/CRC; 2007.
61. Devipriya G, Kalaivani K. Optimal control of multiple transmission of water-Borne diseases. *Int J Math Math Sci.* 2012;2012. ID 421419.
62. Madhu K, Al-arydah M. Optimal vaccine for human papillomavirus and age-difference between partners. *Math Comput Simulation.* 2021;185:325–346. <http://dx.doi.org/10.1016/j.matcom.2021.01.003>,
63. Al-Arydah M, Malik T. An age-structured model of the human papillomavirus dynamics and optimal vaccine control. *Int J Biomath.* 2017;10(6):1750083.